Ocean Engineering 286 (2023) 115587

Contents lists available at ScienceDirect

Ocean Engineering

journal homepage: www.elsevier.com/locate/oceaneng

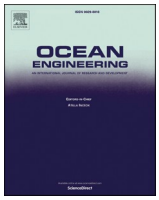

Dynamic response analysis of a monopile-supported offshore wind turbine under the combined effect of sea ice impact and wind load

Ming Song [a], Zhiyu Jiang [b,*], Kun Liu [a], Yue Han [a], Renwei Liu [a]

[a] School of Naval Architecture and Ocean Engineering, Jiangsu University of Science and Technology, Zhengjiang 212003, China
[b] Department of Engineering Sciences,University of Agder, N-4898 Grimstad, Norway

ARTICLE INFO

Keywords:
Drifting ice
Impact load
Wind load
Finite element model
Monopile foundation
Dynamic response

ABSTRACT

The existence of drifting ice is a key challenge for structural design of offshore wind turbines (OWTs) in cold regions. To better understand the structural behavior of OWT under combined sea ice impact and wind load effects, this paper investigates the dynamic response of a monopile-supported OWT using the nonlinear finite element method. The interaction between the OWT and ice impact, wind loads and soil contact are addressed in the developed numerical models in LS-DYNA. The coupling between the main program and the aerodynamic damping model is achieved by a user-defined load subroutine. To calibrate and verify the ice material model and the simulation technique, model test data are used of ice impacts with a nearly vertical monopile foundation. In the case study, numerical simulations of the interaction between a typical 5-MW monopile-supported OWT and an ice sheet are performed under various combined load scenarios. The dynamic response characteristics are presented and the effects of ice drifting speed and mean wind speed are elucidated by statistical methods. Finally, insights into the ice loads are obtained by comparing the simulation results against two international design standards. The present study contributes to an improved understanding of load effects of monopile OWTs in cold regions.

1. Introduction

Offshore wind energy has become a promising source of renewable energy after decades of development. Today, more than 10 European countries have constructed offshore wind farms. The offshore wind capacity installed in the Baltic Sea is 2 gigawatt (GW), and is expected to rise to 85 GW by 2050 (WindEurope, 2019). Fig. 1 shows the average ice coverage of the Baltic Sea during the winter between 1961 and 1990. The maximum extent of ice coverage was 204 000 km^2 during this period (ISO 19906, 2019). The sea ice in this area would bring major challenges for structural design and operation of OWTs (Määttänen, 2010) In addition to other environmental loads like wind and waves, ice loads may induce dynamic vibration and structural failure in the support structures of OWTs.

During an interaction between an offshore structure and a drifting level ice, various failure modes of ice could take place: bending, buckling, cracking/splitting or crushing. These failure modes depend on the shape of the structure at the water level. The sloping shapes cause the level ice to fail by bending, whereas the vertical shapes cause the level ice to fail by crushing. The ice loads due to crushing are higher than those due to other failure modes (Sanderson, 1988), and ice crushing may induce severe steady-state vibrations as well. Therefore, ice crushing can be regarded as the most important failure for the support structure design of OWTs.

There exist various international standards that provide guidance for the design of offshore structures in arctic and cold regions, *e.g.,* ISO 19906 (2019), International Electrotechnical Commission (2019), CAN/CSA S471-04 (2004), API (1995). According to the classification in ISO 19906 (2019), the ice crushing mode can be divided into three categories, namely intermittent ice crushing at a low ice velocity, frequency lock-in crushing at a moderate ice velocity, and continuous brittle crushing at a high velocity. Among them, the continuous brittle crushing is also important for ultimate limit state and fatigue limit state (FLS) designs of structures. The ice-related parameters and ice actions associated with continuous ice crushing on steep and vertical offshore structures are described in this standard. The IEC standard (International Electrotechnical Commission, 2009) provides recommendations for predictions of ice loads for a moving ice sheet on OWT structures with vertical cylindrical shapes. The magnitude of the ice load depends on ice conditions and the size and form of the support structure. Both

* Corresponding Author
E-mail addresses: songmingcssc@163.com (M. Song), zhiyu.jiang@uia.no (Z. Jiang).

https://doi.org/10.1016/j.oceaneng.2023.115587
Received 30 May 2023; Received in revised form 30 June 2023; Accepted 8 August 2023
Available online 24 August 2023

Fig. 1. Baltic Sea ice coverage during winter (from year 1961 to year 1990).

static and dynamic load models are included. However, different standards provide different empirical formulas for prediction of maximum ice loads, and a thorough comparison among these formulas for realistic load cases is lacking.

Many studies have been performed to investigate the ice loads and ice-induced vibrations of vertical offshore structures under crushing failure (Zhu et al., 2020; Yue et al., 2009; Määttänen et al., 2011;Gürtner et al., 2009). Berg et al. (2022) conducted basin tests with a vertical sided cylindrical pile loaded by ice that fails in the crushing mode. Intermittent crushing, frequency lock-in and continuous brittle crushing were observed in the tests. Hendrikse and Nord (2019) proposed a model to simulate the dynamic interaction between a drifting ice floe and a vertically sided offshore structure. The effect of ice floe size and ice drift on the interaction between ice and structure was studied. Kuutti et al. (2013) simulated ice crushing against a rigid vertical structure using the cohesive element method.

Some researchers have focused on the interaction between sea ice and OWTs (Barker et al., 2005; Barooni et al., 2022; Seidel and Hendrikse, 2018). Song et al. (2019) simulated the interaction between level ice and wind turbine tower using the finite element method (FEM). The study confirmed that both mesh size and failure strain of the ice model play a significant role in the simulated ice forces. Ji and Yang (2022) developed a coupled DEM-FEM method to simulate the interaction between the sea ice and the monopile structure of OWT. The sea ice and OWT were simulated through spherical particles in a parallel bonding mode and using the Euler-Bernoulli beam element, respectively. However, the wind loads and local structural deformation were not considered in these studies. Zhu et al. (2018) and Li et al. (2020) investigated the dynamic behavior of pipes subjected to lateral impact loadings, in which the global and local deformations were focused on.

For an operating OWT, wind loads are the primary external loads. A few studies have taken into account the coupling between the ice loads, the wind loads and the dynamic structural response of an OWT under an ice sheet impact. For example, Heinonen and Rissanen (2017) carried out a coupled-crushing analysis of a sea ice-wind turbine interaction. The coupling between the ice, wind and structural response were taken into account. However, the ice model used in the simulation has limited capability to describe brittle crushing of ice. Hammer et al. (2023) investigated the interaction of an idling and operational 14 MW turbine with ice using both the experimental and numerical methods. It was found that multi-modal interaction and intermittent crushing lead to the largest bending moments in the support structure. Shi et al. (2023) performed a numerical study of ice-induced loads and response of a monopile-type OWT. Both wind loads and ice loads were considered in the coupled analyses. However, few studies have focused on the local structural dynamic responses behavior during the OWT-wind-ice interactions. Interesting responses include local deformation of structures, stress distribution, and energy dissipation. As a contribution to new knowledge, there is a strong need for an investigation of local structural response of OWTs under the ice impact and wind load effect.

The objective of the present study is to investigate both the global and local structural dynamic responses behavior of a monopile-supported OWT under an ice sheet impact and wind load effect. This paper considers ice-, wind- and soil-structure interactions simultaneously using the nonlinear FEM. The initial structural response in the continuous brittle crushing mode is focused on. The interaction between an ice sheet and an OWT is simulated in the LS-DYNA software (Hallquist, 2013). In the case study, the NREL 5-MW OWT supported by a monopile foundation and the head-on impact scenario is considered. The ice material parameters are selected corresponding to ice conditions in the Southern Baltic Sea by varying the ice drifting speed. The load cases are selected on the basis of the recommendations from the IEC standard. In addition, a comparison is carried out of the simulated ice loads against the predictions of ice load using the ISO and IEC standards. The contribution of this paper is three-fold. First, a high-fidelity numerical model is developed to capture the global and local structural behavior of OWTs under combined load effects. Second, a fundamental understanding is gained regarding the effect of ice drifting speed and mean wind speed on various response variables. Third, practical discussions are provided for assessment of the maximum ice loads in the context of design standards. The last point is particularly beneficial for design of OWTs in cold regions.

The layout of the paper is arranged as follows. Section 2 describes methodology of the numerical method. Section 3 presents calibration of the ice material model. Section 4 presents case study of a 5-MW monopile wind turbine under ice impact. Section 5 and Section 6 present results and discussions, respectively. Finally, conclusions are drawn in Section 7.

2. Numerical method

This section details methodology of the numerical method, including analysis procedure, modeling of ice-structure interaction, aerodynamic loads and soil-structure interaction.

2.1. Analysis procedure

The interaction between an ice sheet and an OWT is simulated in the main program in LS-DYNA software. The interaction between wind loads and structural response is taken into account by introducing an aerodynamic damping model. The coupling between the main program and the aerodynamic damping model is made possible by means of a user-defined load subroutine (LOADSETUD).

The flowchart of analysis procedure is shown in Fig. 2. The wind loads and the aerodynamic damping for the mean wind speed are precalculated by using the HAWC2 code (Larsen and Hansen, 2018). The ice-structure interaction model includes both ice and OWT finite element models, and the wind loads are applied on the tower top. During the time-domain simulation, LS-DYNA calculates ice loads, motion response and structural response, and passes information of the nodal velocity for the current time step to the user subroutine. The selected node is the one at the tower top. The nodal velocity history is stored, and the aerodynamic damping force related to velocity is calculated in the user load subroutine. The obtained aerodynamic damping force is applied on the tower top, and LS-DYNA then calculates the results, and

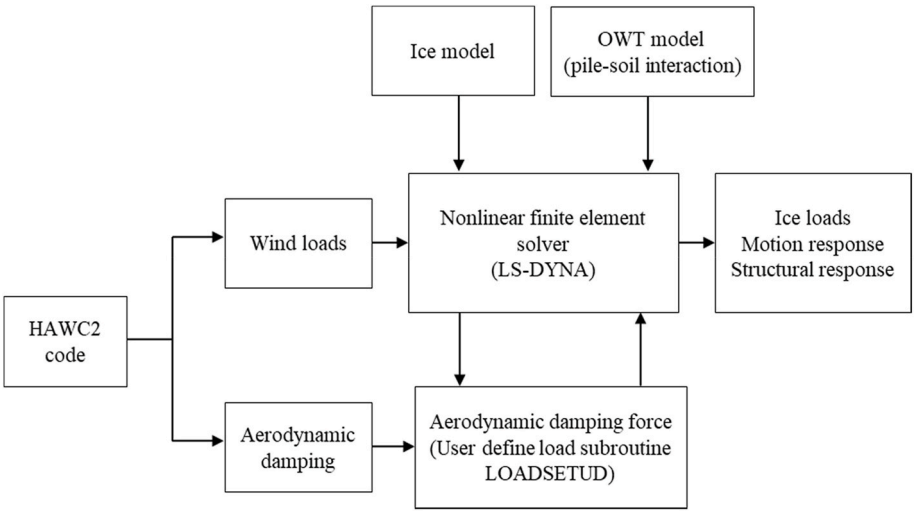

Fig. 2. Flowchart of the analysis procedure.

provides information of the tower-top motion for the next time step. Previously, this approach was adopted (Song et al., 2021) for simulating the load effects of an OWT under ship collisions.

2.2. Modeling of ice-structure interaction

During the ice-structure interaction, the dynamic structural response of an OWT is analyzed using the nonlinear finite element method based on explicit time integration. The equations of motion can be expressed as:

$$\boldsymbol{M}\ddot{U} + \boldsymbol{C}\dot{U} + \boldsymbol{K}U = \boldsymbol{F} \tag{1}$$

where $\boldsymbol{M}$ is the diagnonal mass matrix, $\boldsymbol{U}$, $\dot{\boldsymbol{U}}$ and $\ddot{\boldsymbol{U}}$ are the displacement, velocity and acceleration vectors, respectively, $\boldsymbol{F}$ accounts for the collision loads and the aerodynamic loads, $\boldsymbol{C}$ and $\boldsymbol{K}$ are the damping matrix and the stiffness matrix, respectively.

Both finite element (FE) models of an OWT and an ice sheet are needed to be built for FE analysis of the ice-structure interaction. The four-node Belytchko-Tsay shell elements with 5 integration points along the thickness are used to model the OWT structures. The eight-node solid elements are used to model the ice sheet. An elastic-plastic material model with the power-law hardening is used for the OWT.

The dynamic structural response of an OWT subjected to sea ice impact is generally associated with ice failure. The failure mode, *e.g.,* crushing, splitting, flexural, for level ice depends on ice thickness, ice drifting speed and structure shape. When an ice sheet impacts with vertical structures, ice crushing is the dominant failure mode. In this study, the impacted monopile-supported OWT has a vertical foundation. Therefore, the isotropic elasto-plastic material model proposed by Hilding et al. (2011) is used for the ice sheet to simulate the crushing failure of ice. The ice material is assumed to be elastic before reaching the initial point during crushing. After the first crack is initiated, the ice material follows a linear softening behavior. When the ice is totally crushed, it behaves as a viscous fluid. This ice model has been validated for describing ice brittle crushing in ice-structure interaction (Song et al., 2019; Wang et al., 2018).

To describe the ice behavior, the "mat-piecewise-linear-plasticity" material type from LS-DYNA's suite of material types is used here, in which an elasto-plastic material with yield stress versus strain curve and failure based on a plastic strain can be defined.

The failure strain of the ice model is not a strictly material property but rather a numerical remedy to excessive mesh distortions within the Lagragian formulation (Song et al., 2016). Its application to the simulation of a physical phenomenon requires the calibration with experimental data.

To avoid initial penetration, a gap is set between FE models of OWT and ice before impact. The translational velocity of ice ramps up from 0.0 m/s to target velocity before the impact occurs, and the velocity is kept to be constant throughout the rest of the simulation.

The contact between the OWT and the ice sheet is implemented using a contact-eroding-surface-to-surface formulation, which is used with the segment-based contact option (soft = 2). The contact-eroding-single-surface is applied for ice model to consider the self-contact of the ice component.

2.3. Modeling of aerodynamic loads

The effect of wind loads is important for an operating wind turbine. During the ice-structure interaction, the aerodynamic loads induced by wind will affect the dynamic response of OWT and structural vibration of the support structures. Therefore, the wind-structure interaction should be taken into account for an operation OWT.

In this study, to represent the wind load effect on an operational OWT, both the aerodynamic damping and the mean thrust force are addressed in the modeling. The linearized aerodynamic damping coefficient can be numerically estimated based on changes in the thrust force due to a change in wind speed without considering the effect of the control system (Bachynski, 2014):

$$c_{aero} = \frac{dF_{Thrust}}{dV_{mean}} \tag{2}$$

where dV_{mean} denotes a small variation in the mean wind speed and dF_{Thrust} denotes the corresponding change in the thrust force. For a range of constant wind speeds, time-domain simulations are carried out in an aeroelastic code for a land-based wind turbine with the blade pitch and rotor speed fixed for each wind speed, and the damping values are estimated accordingly. Note that Eq. (2) is only valid for operating wind turbines. For parked (standing-still or idling) wind turbines, the mean wind loads and aerodynamic damping are deemed small.

In this work, the values of wind loads and aerodynamic damping coefficient are calculated using the HAWC2 software based on the blade element momentum theory. To ensure a gradual loading without generating any transient effects, the calculated mean values of wind loads and moments under steady wind conditions are applied on the tower top by using progressive loading curves. The aerodynamic damping force equivalent to $c_{aero} \times V_{vib}$ is implemented in the user load subroutine. Here, V_{vib} is the vibration-induced velocity of the tower-top node.

2.4. Modeling of soil-structure interaction

The monopile foundation of an OWT is flexible due to the effect of soil. To take into account this flexibility of foundation, the soil-structure interaction is included in this study.

Typical soils such as sand or clay generally behave as a plastic material under static lateral loading, which results in nonlinear relationship between soil resistance p and pile/soil deflection y. The design in the Offshore Code Comparison Collaboration (OC3) project for the International Energy Agency (IEA) used the nonlinear p-y model for sand which depends on the effective weight, angle of internal friction of the sand, pile diameter and local soil depth (Jonkman et al., 2007). For dynamic analysis, most codes use the simplified linear foundation models, such as the apparent fixity model, coupled springs model and distributed springs model.

In this study, the distributed springs model is used, in which lateral springs are distributed along the subsoil portion of monopile; see Fig. 3. The OWT structures use the real properties of the monopile both above and below the mudline, including the real penetration depth. The subsoil spring stiffness constants are depth-dependent and are calculated on basis of a linearization of the p-y model.

3. Calibration of the finite element models based on model tests of ice-OWT interaction

For assessment of structural response subjected to an ice sheet impact, it is important to represent the ice forces accurately. In order to calibrate and validate the performance of the FE models with selected parameters such as element size and failure strain, previous model test results of ice-OWT interaction are used.

3.1. Model tests of ice-OWT interaction

The model tests were conducted by Wu et al. (2018) at the ice Basin of Tianjin University. The ice tank is 40.0 m long, 6.0 m wide and 1.8 m deep. The tests represent impacts between an ice sheet and monopile foundation of a 3-MW wind turbine. The test scale was 1:20. The geometry of the monopile foundation at full scale is shown in Fig. 4. The foundation has nearly vertical structure and the diameter at the waterline is 5.30 m at full scale, and its inclination angle is 87.2°. One selected experimental scenario from the model test for the 3-MW OWT is shown in Fig. 5. The interaction between the ice and the structure was conducted by moving the OWT with a trailer. The impact speed was set by controlling the speed of the trailer. A force transducer was installed to measure the ice forces using a data acquisition system at a sampling frequency of 100 Hz.

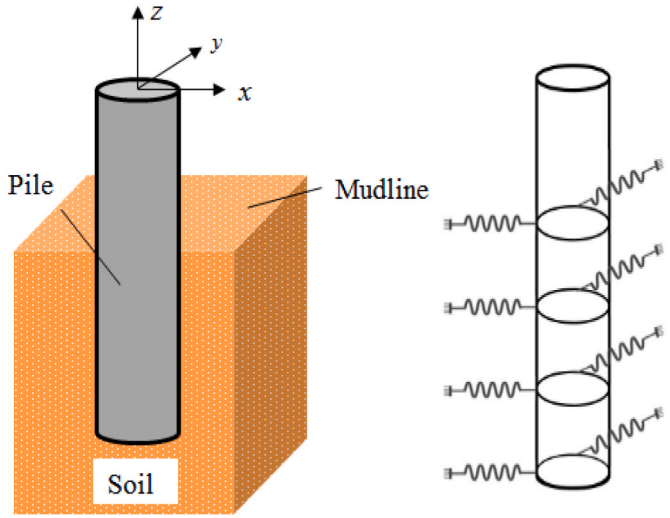

Fig. 3. Illustration of the distributed springs model for a monopile.

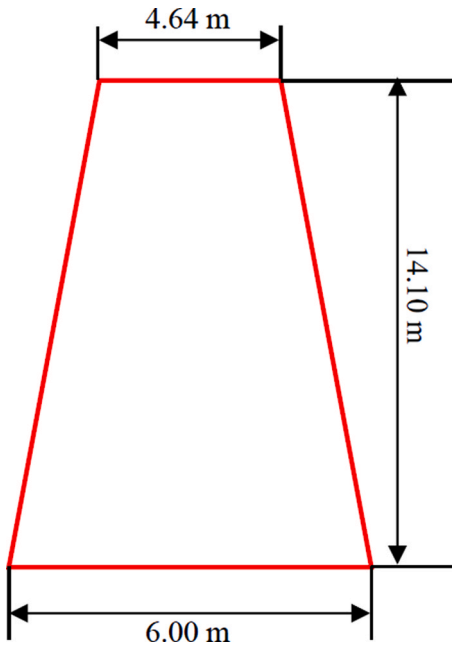

Fig. 4. Full-scale geometry of monopile for the 3- MW OWT.

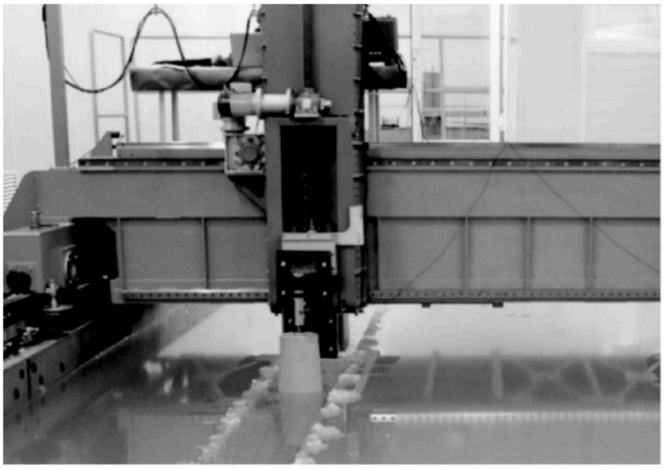

Fig. 5. Photograph of the model test for the 3-MW OWT (Wu et al., 2018).

In the tests, the target ice thickness h is 0.4 m (full-scale), and the compression strength of the ice is approximately 2.06 MPa (full-scale). The impact speed V_{ice} is 0.6 m/s. The crushing failure mode of the brittle ice took place in the test.

3.2. Sensitivity study of mesh size and failure strain in finite element modeling

Numerical simulations of the collisions between the ice sheet and the 3-MW OWT are performed. The input parameters of the numerical simulation are kept the same as those of the model tests. The OWT is assumed to be rigid. The mesh size of the OWT is approximately 0.2 m × 0.2 m. The ice material model presented in Section 2.1.2 is used and the input material parameters are set based on the measurements in the model test. The ice density is taken to be 900 kg/m^3, the Young's

modulus is taken to be 2 GPa, and the yield stress is taken to be 2.06 MPa. For the ice, four meshes with characteristic element lengths of 0.2 m, 0.4 m, 0.6 m and 0.8 m are considered. The corresponding values of failure strain are determined based on trial and error (see Table 1).

Table 1 shows a comparison of the statistics obtained from the simulated and measured time series. For the maximum ice force, the numerical simulations with different mesh sizes and failure strains predict reasonable results, and the largest difference between the simulated and test results is 6.7%. For the mean force, the magnitude is observed to increase as the mesh size decreases. A mesh size of 0.4 m should be considered to ensure a good comparison against the measurements, in which the relative error of the mean ice force between the simulation and model test is 1.7%. Generally, the standard deviation (STD) obtained from the simulations is higher than that from the model test.

Fig. 6 shows the ice load acting on the 3-MW OWT obtained from the model test and numerical simulation with a mesh size of 0.4 m and a failure strain of 0.29. It is found that there is a good agreement between the simulated and measured results, in which both the ice loads present considerable oscillations around the mean value. However, the simulated fluctuation frequency and STD are slightly higher than the measured values. This is mainly because the high-frequency component in the signal was filtered out during the transformation from the model test data to the field ice force (Ji and Yang, 2022).

Overall, the ice material model with the mesh size (0.4) and failure strain (0.29) give accurate results. These parameters will be considered in the case study of this work.

4. Case study

4.1. Description of the offshore wind turbine model

The NREL-5 MW wind turbine supported by a monopile foundation (Jonkman et al., 2007) at 20 m water depth is considered in this study. The OWT has a rotor-nacelle assembly mass of 350 t. The OWT structure consists of three main parts: a monopile, a transition piece, and a tower. The main properties are presented in Table 2.

As the nacelle and rotor blades of the OWT are far from the contact area, their effects on the monopile's structural response can be neglected. Thus, to simplify the FE modeling, this rotor-nacelle system is replaced by a lumped mass located at the top of the tower. A fine mesh with a size of 0.2 m is used for the contact area. To reduce the computational time, a coarse mesh size of 0.5 m is applied to the rest of the monopile structure. The total number of the shell elements for the OWT model is 29,768. The effective density of the OWT is taken to be 8500 kg/m^3 to account for paint, bolts, welds and flanges that are not considered in the wall thickness data. For the steel material, the yield stress is 355 MPa, the Young's modulus is 207 GPa, and the plastic failure strain is 0.3. The strength coefficient is 760 MPa and hardening exponent is 0.225, respectively.

This simplified OWT model has been verified by comparing the lowest natural frequencies with those of full rotor system (Song et al., 2021). The results obtained by the modal analysis of the simplified OWT model match those of the full rotor system predicted by the HAWC2 code. Refer to Song et al. (2021) for details.

Table 1
Comparison between the simulated and measured results for the model test.

Items	Numerical Simulations (MN)				Model Test (MN)
	Mesh size/ failure strain 0.2 m/0.43	Mesh size/ failure strain 0.4 m/0.29	Mesh size/ failure strain 0.6 m/0.17	Mesh size/ failure strain 0.8 m/0.14	
Maximum	3.48	3.34	3.27	3.35	3.49
Mean	1.58	1.17	0.93	0.74	1.15
STD	0.66	0.72	0.68	0.83	0.60

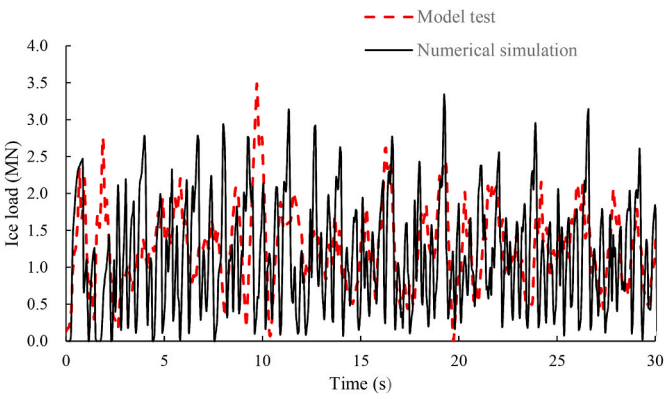

Fig. 6. Comparison between the model test and numerical simulations (with a mesh size of 0.4 m and a failure strain of 0.29).

Table 2
Main parameters of the OWT.

Item	Value
Water depth (m)	20
Monopile diameter (m)	6
Monopile thickness (mm)	60
Transition diameter (m)	6
Transition thickness (mm)	60
Tower base diameter (m)	6
Tower base thickness (mm)	27
Tower top diameter (m)	3.87
Tower top thickness (mm)	19.4
Tower height (m)	77.6
Rotor-nacelle assembly mass (t)	350
Cut-in, rated, and cut-out wind speed (m/s)	3, 11.4, 25

4.2. Description of the ice sheet model

The ice conditions typical of the Baltic Sea are specified by the ISO standard (2019) and an ice thickness h of 0.4 m is considered in this study. The dimensions of the ice are 80 m × 60 m × 0.4 m. This dimension is sufficient to minimize the effect of boundary conditions. The eight-node solid elements are used with a mesh size of 0.4 m × 0.4 m × 0.4 m. The number of elements for the ice is 22,500. The ice density is 880 kg/m^3, the Young's modulus is 5.4 GPa, the yield stress is 2.3 MPa, and the failure strain is 0.29.

4.3. Load cases

According to design load cases for sea ice suggested by International Electrotechnical Commission (2019), 10 collision cases are simulated; see Table 3. The ice thickness h is 0.4 m. The wind speed V_{wind} varies from 0 m/s to 25 m/s. For the OWT, both parked and operating

Table 3
Load cases for the OWT under the combined loads of wind and ice.

Load case	h (m)	V_{ice} (m/s)	V_{wind} (m/s)	Turbine state
1	0	0	11.4	Operating
2	0.4	0.3	11.4	Operating
3	0.4	0.4	11.4	Operating
4	0.4	0.5	11.4	Operating
5	0.4	0.6	11.4	Operating
6	0.4	0.7	11.4	Operating
7	0.4	0.5	0	Parked
8	0.4	0.5	8	Operating
9	0.4	0.5	17	Operating
10	0.4	0.5	25	Operating

conditions are considered. To investigate the effect of ice drifting speed V_{ice} on the structural response, the ice drifting speeds varying from 0.3 m/s to 0.7 m/s are considered. A schematic diagram of the ice-OWT interaction is shown in Fig. 7. In this work, the head-on impact scenario is focused on.

4.4. Wind loads and aerodynamic damping coefficients

Table 4 presents the mean values of the wind loads and moments, and the aerodynamic damping coefficients under steady wind conditions with different wind speeds. It is observed that F_y initially rises along with the increase of wind speed and the highest value is attained at the rated wind speed (11.4 m/s), and then F_y decreases with the increase of wind speed. This trend is expected given the operational characteristics of the wind-induced thrust. The obtained wind loads and moments are applied on the tower-top node by using progressive loading curves.

5. Results

5.1. Convergence study of the simulation length

According to International Electrotechnical Commission (2019), the simulation length should be long enough to account for the stochastic uncertainties before a reliable estimate of the characteristic load effect can be achieved. In general, at least 10-min simulation length is required for the dynamic ice load. However, it is computationally prohibitive to simulate the ice-structure interaction for such a long length using the high-fidelity nonlinear finite element method. As the size of ice sheet depends on the ice drifting speed and the simulation length, an increase in the simulation length results in a substantial increase in the number of ice elements. Considering the current best practices (Ji and Yang, 2022), it is desirable to shorten the simulation time while having statistically meaningful results.

To this end, a convergence study on the numerical simulation length for the coupled dynamic analysis under wind and ice loads is carried out. Three different simulation lengths (40 s, 80 s, 120 s) are investigated. In these simulations, the ice drifting speed is 0.3 m/s and the wind speed is 11.4 m/s. The results including the mean and STD of the ice loads are presented in Table 5. It is seen that the differences for both statistics are relatively small when the simulation length is larger than 40 s. Considering the trade-off between the computational time and the result accuracy, a simulation length of 40 s is selected in the simulations of the load cases.

Table 4
The wind loads and aerodynamic damping coefficients under different mean wind speeds (Refer to Fig. 7 for the coordinate system).

V_{wind} (m/s)	0	8	11.4	17	25
F_x (kN)	0	2.4	6.9	8.2	11.2
F_y (kN)	0	399.5	644.5	365.9	278.6
F_z (kN)	0	−37.0	−55.9	−27.5	−7.8
M_x (kNm)	0	1232.0	1096.6	1020.5	618.0
M_y (kNm)	0	1998.5	3895.6	3865.0	3813.3
M_z (kNm)	0	−272.7	−756.1	−1095.4	−1686.1
c_{aero} (kNs/m)	0	66.6	90.4	75.7	67.7

Table 5
Comparison of the ice loads for different simulation lengths.

Simulation length (s)	Mean (MN)	STD (MN)
40	1.38	0.71
80	1.39	0.69
120	1.38	0.71

5.2. Dynamic response induced by ice loads

The dynamic response of the OWT under different load cases is investigated. In case 1, the OWT under only wind loads for a mean wind speed of 11.4 m/s is considered. In case 4, the OWT in the operating condition with a mean wind speed of 11.4 m/s and the ice sheet with a thickness of 0.4 m and a drifting speed of 0.5 m/s are assumed. In case 7, the OWT in the parked condition with a zero wind speed, and the same ice conditions in case 4 are assumed.

5.2.1. Ice load characteristics

Fig. 8 shows the time history of the ice load for case 4 with a mean wind speed of 11.4 m/s and a drifting ice speed of 0.5 m/s. It is seen that

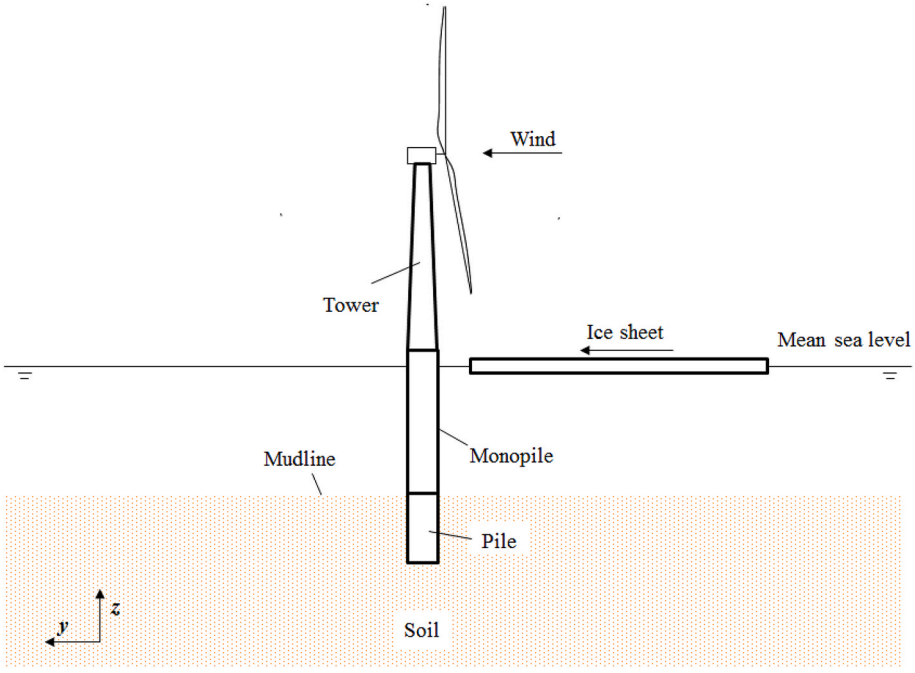

Fig. 7. Schematic of the head-on impact scenario between an ice sheet and an OWT.

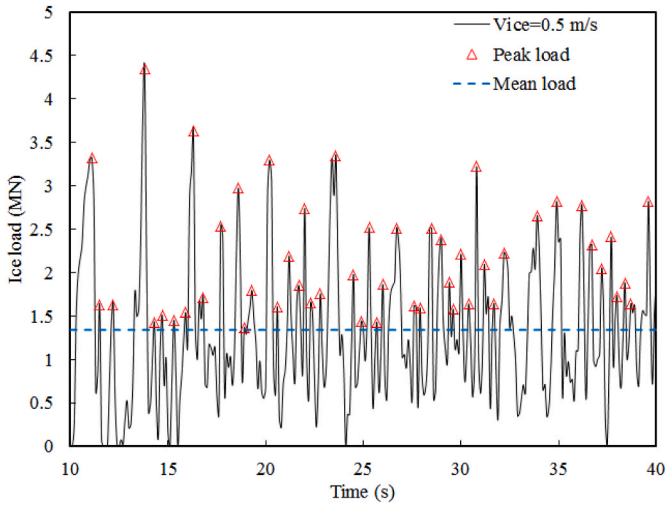

Fig. 8. Time history of the ice load for case 4.

the ice loads are random as continuous brittle crushing takes places. To estimate the extreme response, the Weibull probability model is applied to fit the response maxima using the least squares method. The cumulative distribution function of the two-parameter Weibull model with scale parameter a and shape parameter b is given as

$$\mathrm{F}(x|a,b) = 1 - \exp\left(-\left(\frac{x}{a}\right)^{b}\right) \tag{3}$$

where F is the cumulative distribution function of the distribution.

As the peak ice load is of interest here, only the individual maxima above the mean value are selected in the probability fitting; these maxima are highlighted in Fig. 8. The sample x of the probability model is calculated from the dynamic loads (peak values minus the mean) of each realization. To assess the selected distribution, the probability paper is employed. Thus, from Eq. (3) we obtain

$$\ln\left[-\ln(1-\mathrm{F}(x|a,b))\right] = b\ln(x) - b\ln a \tag{4}$$

We can rewrite this equation on the form

$$y = bz + c \tag{5}$$

where $y = \ln[-\ln(1-\mathrm{F}(x|a,b))]$, $z = \ln(x)$ and $c = -b\ln a$.

The fitted dataset of one representative load case (case 4) is shown in Fig. 9. It is observed that the data from the presented simulation form nearly a straight line, which indicates that the Weibull model reasonably fits the data. In particular, the data in the upper tail region appear to lie on the line. The present estimation of extrema is regarded as a short-term statistics for a time history. To derive the extreme values corresponding to a small probability of exceedance with a certain return period, a comprehensive long-term analysis is needed that considers the probability of occurrence of different ice/wind conditions. Upon availability of such information, such long-term analysis may be pursued in future.

Fig. 10 shows the power spectrum density of the ice forces for case 4 after a fast Fourier transform. It is found that the main energy is concentrated in the low-frequency region, which covers the first fore-aft (F-A) natural frequency (0.24 Hz) of the OWT. A minor peak may be seen in the force spectrum at the resonance frequency of the OWT. This finding is similar to that in Gravesen et al. (2005) for analysis of the measured force on the cylinder during a continuous crushing failure.

5.2.2. Tower motion response

Fig. 11 shows the tower-top displacement histories in the F-A direction for different cases. The ice sheet impact takes place around 10 s. For case 4 with combined ice impact and wind loads, the tower-top displacement increases significantly due to the ice loads at the initial transient stage. Then, the amplitude decays rapidly due to the effects of the aerodynamic damping. Higher maximum and mean tower-top displacement and more oscillations are found in this case than in cases 1 and 7. The maximum value of tower-top displacement is 1.22 m in the case considering combined ice impact and wind loads, which is approximately 2.58 times than that for case 7 which considers only the ice loads (0.47 m), and 1.47 times than that for case 1 which considers only the wind loads (0.83 m). The simulation with parked wind turbine yields much larger amplitudes of the tower vibration due to lack of aerodynamic damping effect. The period of the tower oscillations after the ice impact is approximately 4.4 s, which is close to the first eigen period of the OWT (4.2 s).

5.2.3. Structural response

Fig. 12 shows the comparison of the bending moment of the OWT in the F-A direction at the mean sea level (MSL) and at the mudline for different cases. The simulation for case 4 results in the largest maximum bending moments at the MSL and at the mudline due to the combined ice impact and wind loads effect. However, there is little difference in the mean bending moment at the MSL between case 1 and case 4 because this bending moment is dominated by the wind loads. This observation

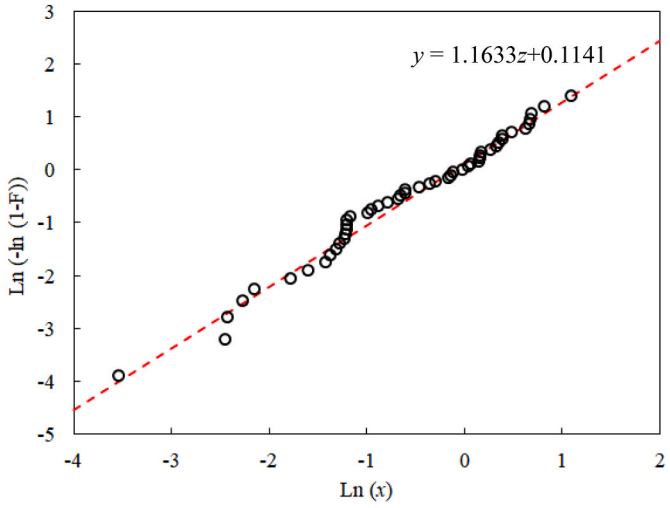

Fig. 9. Fitted peak ice load for case 4 on the Weibull probability paper.

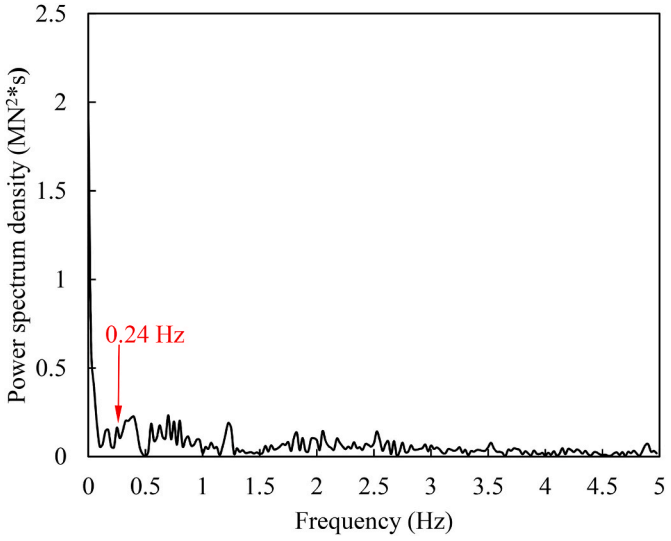

Fig. 10. Power spectrum density of the ice force for case 4.

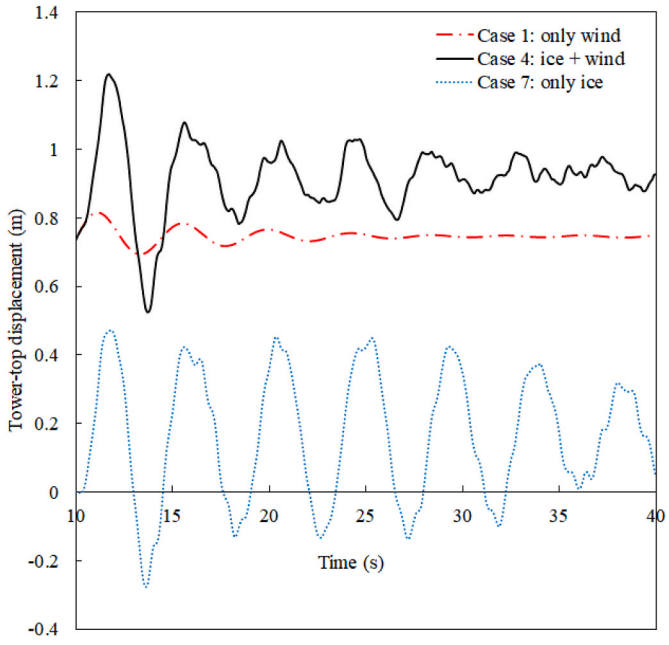

Fig. 11. Tower-top displacement histories for different cases.

is aligned with the result obtained with considering only ice loads, in which the mean bending moment at the MSL is small. The maximum and mean values of the bending moment are 135.2 MNm and 97.8 MNm for the case with considering combined ice impact and wind loads, which are 1.72 and 1.36 times than those of the only wind loads, and are 1.69 and 3.74 times than those of the only ice loads. In addition, the standard deviations of the bending moment at the MSL and at the mudline for the cases with considering ice loads are much larger than those obtained with considering only wind loads. This may significantly affect the fatigue damage which is associated with cyclic loading.

Fig. 13 shows the time history of effective stresses, *i.e.*, von Mises stress, of the OWT under combined sea ice impact and wind loads. Initially, the maximum structural stress locates at the center of contact area. The value of maximum structural stress reaches 337.4 MPa, which is slightly lower than the yield stress (355 MPa) of the OWT. This high stress is due to high loading caused by the intact ice sheet impact. Around 20 s, there is a gap between the OWT and the ice sheet, which results in lower load and consequently lower stress (the maximum stress is 144.0 MPa). This gap is mainly caused by the ice breaking and the motion of the OWT. The simulated ice breaking length depends on the mesh size of the ice. Both the global and local deformations of the OWT occur due to the ice loads effect. With the forward movement of the ice, the continuous interaction between the OWT and the ice take places. Around 32.8 s, the maximum structural stress of 276.7 MPa is obtained.

5.3. Dynamic response under the rated wind speed and varying ice drifting speed

To investigate the influence of the ice drifting speed, we vary the speed from 0.3 m/s to 0.7 m/s for different ice-OWT collision cases. The mean wind speed is fixed as 11.4 m/s (rated speed) and the thickness of ice sheet is assumed to be 0.4 m.

5.3.1. Ice loads

The variations of the ice loads for an ice drifting speed of 0.3 m/s and 0.7 m/s are depicted in Fig. 14. It is seen that these ice loads are random. There is a large change in the ice-breaking period. This is because the ice breaking period is dominated by the ice drifting speed.

Table 6 presents the maximum, mean and standard deviation of the ice loads for different ice drifting speeds. The maximum ice load initially increases as the ice drifting speed increases and the highest value is attained when the ice drifting speed is 0.5 m/s. There is no large difference between the cases for a larger speed (0.5 m/s-0.7 m/s). This feature has also been observed in model tests (Gravesen et al., 2005; Wu et al., 2018). In addition, a negligible drifting speed effect on the mean ice force is found.

5.3.2. Tower motion response

A comparison of the tower-top F-A displacement for different ice drifting speeds is shown in Fig. 15 and Table 8. During the initial response to the ice impact, there are significant peak and period differences in the tower oscillation. These differences are caused by the peak and duration differences in the initial ice forces (see Fig. 14). However, there is no large difference in the tower-top displacement after the 30 s. In Table 7, it is seen that the maximum and standard deviation of the tower-top displacement decrease as the ice drifting speed increases. This is because lower ice drifting velocity causes higher ice load and longer duration for the initial impact phase, and consequently results in greater initial structural vibration. But there is little difference in the mean value of tower-top displacement. This is because the effect of the ice drifting speed on the mean ice force is small. It can be concluded that the ice drifting speed has a significant effect on the tower-top displacement at the initial stage the ice-OWT impact. However, this effect can be neglected after the initial stage, *i.e.*, around 30 s.

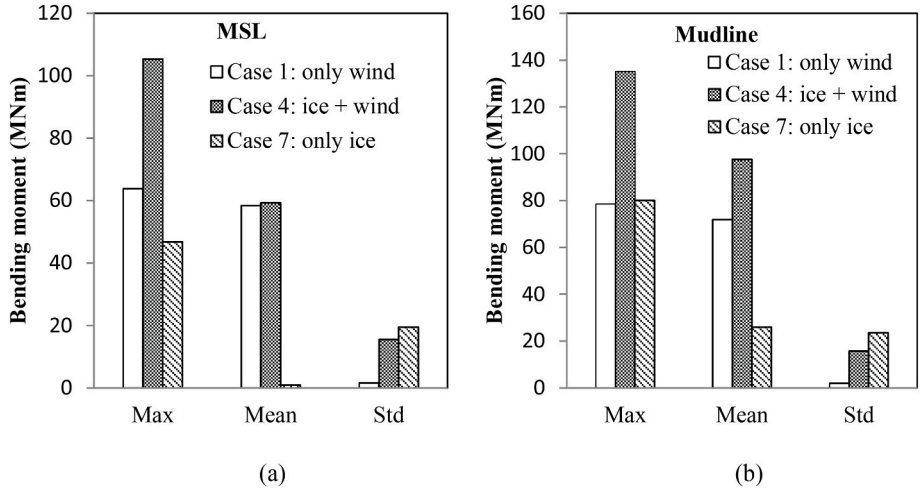

Fig. 12. Comparison of the monpile F-A bending moment under different cases: (a) at the MSL and (b) at the mudline.

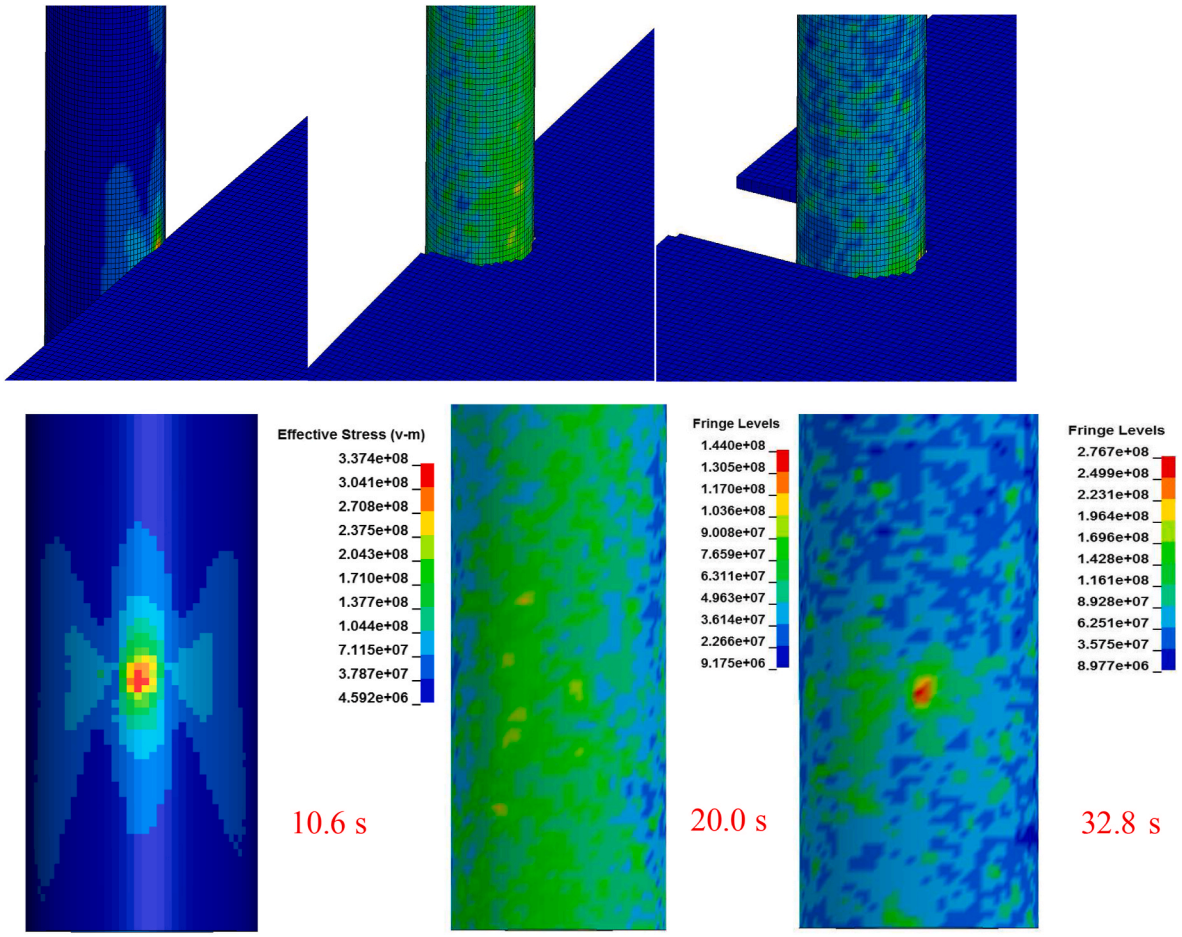

Fig. 13. Time history of stresses of the OWT impacted by an ice sheet with a velocity of 0.5 m/s.

Large acceleration at the top of the OWT will result in a risk for the electrical equipment of the wind turbine. The maximum allowable acceleration of the nacelle is 6 m/s^2 according to Siemens Gamesa (Liu et al., 2015). Therefore, it is necessary to evaluate the tower-top acceleration under the ice impact. The maximum tower-top F-A acceleration with respect to the ice drifting speed is shown in Fig. 16. It is seen that the maximum tower-top accelerations for these cases range from 2 m/s^2 to 2.7 m/s^2, which is below the maximum allowable acceleration.

5.3.3. Structural response

Fig. 17 shows the bending moment in F-A direction at the mudline with respect to ice drifting speed. It is observed that the effect of the ice drifting speed on the mean bending moment at the mudline is minimal. This finding is similar to that in Shi et al. (2016) who simulated the interaction between ice and a monopile-type OWT with a downward ice-breaking cone. The maximum bending moment at the mudline for different ice drifting speeds ranges from 145 MNm to 164 MNm, and the standard deviation ranges from 16 MNm to 21 MNm. The difference in the maximum bending moment at the mudline for different ice drifting speeds is within 13%.

5.3.4. Internal energy

During the ice-structure interaction, the internal energy absorbed by the OWT structures includes both elastic deformation energy and plastic deformation energy due to the combined ice impact and wind loads. The internal energy histories of the OWT for different ice drifting speeds are compared in Fig. 18. Around 10 s, the values of the internal energy of the OWT for different ice drifting speeds are the same. This is because the internal energy is stored as elastic deformation energy in the OWT due to the wind loads before the ice impact. After the ice impact, the internal energy increases rapidly. It is seen that there are obvious fluctuations during the ice-OWT interaction, and the peaks and valleys of the internal energy are in good correspondence with those of the tower-top displacement. This is because the structural flexibility the OWT is considered in the simulation and both the global and local oscillations of the OWT are induced by the ice impact. Around 40 s, the values of the energy dissipated by the OWT for an ice drifting speed of 0.3 m/s, 0.5 m/s and 0.7 m/s are 0.57 MJ, 0.76 MJ and 0.89 MJ, respectively. The total energy dissipated by the OWT increases with the increase of ice drifting speed. This is because there is high impact kinetic energy for large ice drifting speed.

5.4. Sensitivity study of the mean wind speed on the dynamic response

To investigate the effect of the mean wind speed, five cases are analyzed in which the mean wind speed varies from 0 m/s to 25 m/s. The wind turbine is in the parked condition when the mean wind speed is equal to zero. The ice sheet has a thickness of 0.4 m and a drifting speed of 0.5 m/s in these cases.

5.4.1. Ice loads

Table 8 presents the maximum, mean and standard deviation values of the ice loads for different mean wind speeds. Largest maximum and standard deviation of the ice load are obtained when the mean wind speed is 11.4 m/s. There are small changes in the maximum ice load (less than 10%), the mean ice load (less than 3%) and the standard deviation (less than 11%) as the mean wind speed increases. It indicates that the influence of the mean wind speed on the ice load can be neglected.

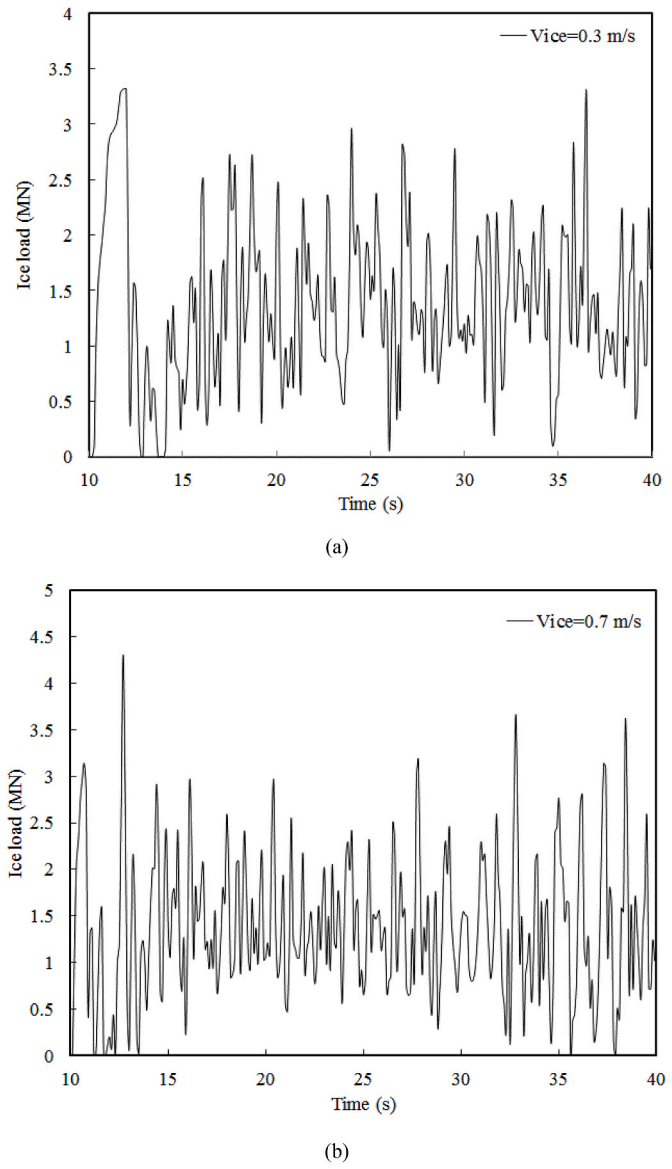

Fig. 14. Time histories of the ice force for different ice drifting speeds: (a) 0.3 m/s, (b) 0.7 m/s.

Table 6
Ice force for different ice drifting speeds.

V_{ice} (m/s)	Max (MN)	Mean (MN)	STD (MN)
0.3	3.32	1.38	0.71
0.4	4.02	1.34	0.82
0.5	4.36	1.34	0.81
0.6	4.14	1.39	0.79
0.7	4.31	1.38	0.76

5.4.2. Motion response

Fig. 19 shows the tower-top displacement histories in the F-A direction for different mean wind speeds. It is seen that the case with a mean wind speed of 11.4 m/s yields much higher tower-top displacement than the other cases. This is because the wind loads (thrust force) are the largest when the mean wind speed is equal to the rated. There is no large difference in the tower-top displacement between the cases for the wind speed of 8 m/s and 17 m/s because the thrust forces (i.e., F_y) under these mean wind speeds are close (see Table 4). The simulation with the OWT in parked condition induces the smallest maximum tower-top displacement. Therefore, the mean wind speed has a significant effect on the tower-top displacement. Ignoring wind loads may underestimate the tower-top displacement.

Fig. 20 shows the maximum tower-top F-A acceleration with respect to the mean wind speed. When the wind turbine is in operating conditions, the maximum tower-top accelerations for the mean wind speed varying from 8 m/s to 25 m/s are approximate 2.0 m/s^2. For the parked wind turbine, *i.e.*, the mean wind speed is 0 m/s, the maximum tower-top acceleration is 2.3 m/s^2, which is slightly larger than those obtained for operating wind turbine. This is due to the lack of aerodynamic damping for the parked wind turbine.

5.4.3. Structural response

Fig. 21 shows the bending moment in F-A direction at the mudline for different mean wind speeds. It is observed that there are significant differences in the F-A bending moment response under different mean wind speed. When the mean wind speed is lower than 11.4 m/s, the maximum and mean F-A bending moment at the mudline rise along with the increase of the mean wind speed, but the standard deviation decreases with the increase of the mean wind speed. When the mean wind speed is equal to 11.4 m/s, the highest maximum and mean values and the lowest standard deviation are attained. For higher mean wind speed, the maximum and mean F-A bending moment at the mudline show a decreasing trend, but the standard deviation shows a slow growth trend. It can be concluded that the mean wind speed has a strong effect on the F-A bending moment at the mudline.

5.4.4. Internal energy

Fig. 22 shows the energy dissipated by the OWT for a mean wind speed of 0 m/s, 11.4 m/s and 17 m/s. Around 10 s, the energy dissipations of the OWT for a mean wind speed of 11.4 m/s and 17 m/s are 0.28 MJ and 0.11 MJ, respectively, which are induced by the wind loads. During the ice-OWT interaction, there are significant differences in the energy dissipation of the OWT. This is mainly due to different motion of the OWT under different wind speeds (see Fig. 19).

5.5. Comparison of the simulation results with design standards

Many international standards or classification rules and guidelines provide empirical formulas to predict ice loads on offshore structures. These formulas are based on assumptions in combination with model or full-scale tests. A comparison between the ice loads obtained by the present simulations under different load cases (cases 2–10) and the predictions using these standards is of interest.

In this study, ISO 19906 (2010, 2019), and IEC 61400–3 ((2009, 2019) standards are chosen. Because ISO 19906 is widely adopted or recommended for ice load calculations by other standards organizations, such as current Canadian CSA Arctic offshore structures, RP 2 N from the API,6)DNVGL-ST-0437 (2016), Norwegian (NORSOK N-003, 2007), and IEC 61 400–3 focuses on design ice loads for OWT support structures. It is noted that the maximum static force due to ice crushing on the vertical cylindrical structures i9)International Electrotechnical Commission (2019) is calculated on basis of the formula i0)ISO 19906 (2010). A comparison of these standards for predicting ice loads from moving ice sheet on vertical structures is summarized in Table 9. The ice load formula in ISO standar,(2010,9) 2019)an9)International Electrotechnical Commission (2019) are based on full-scale measurements in Cook Inlet, the Beaufort Sea, Baltic Sea and Bohai Sea, but the ice load formula in IEC standar9)International Electrotechnical Commission (2009) is based on measurements from model tests and fresh water ice in rivers (Kellner et al., 2017).

When ice crushing occurs against a vertical structure, ISO 19906 standards (2010, 2019) and International Electrotechnical Commission (2019) recommends the following global ice load as

$$F_G = p_G h w \tag{6}$$

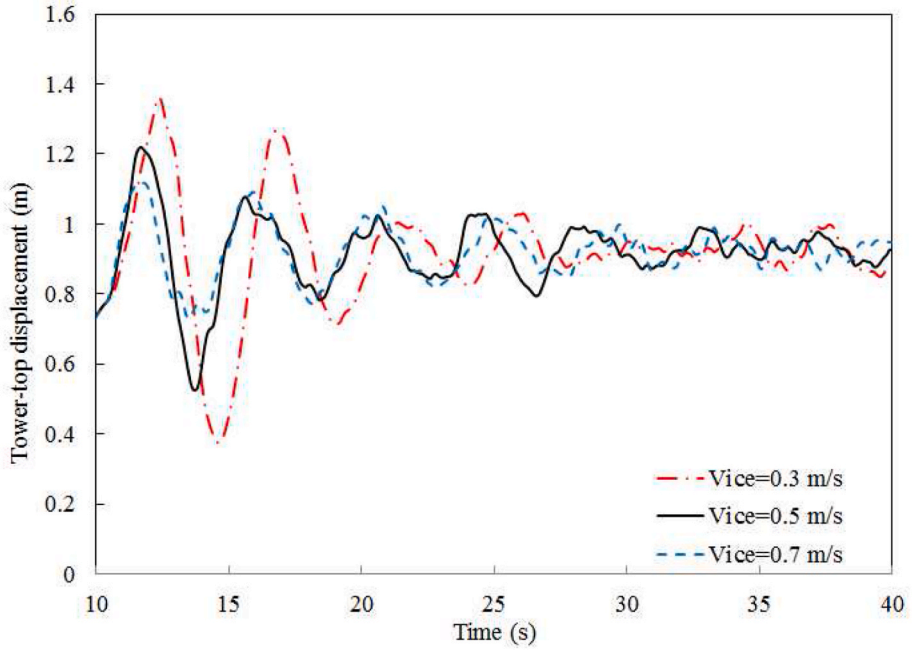

Fig. 15. Time histories of the tower-top F-A displacement for different ice drifting speeds.

Table 7
Tower-top F-A displacement under different ice drifting speeds.

V_{ice} (m/s)	Max (m)	Mean (m)	STD (m)
0.3	1.36	0.92	0.16
0.4	1.27	0.92	0.15
0.5	1.22	0.92	0.10
0.6	1.15	0.93	0.07
0.7	1.12	0.92	0.08

Table 8
Ice force for different mean wind speeds.

V_{wind} (m/s)	Max (MN)	Mean (MN)	STD (MN)
0.0	4.04	1.35	0.78
8.0	4.08	1.36	0.75
11.4	4.36	1.34	0.81
17.0	4.12	1.33	0.73
25.0	3.96	1.34	0.77

where h is the ice thickness, w is the structure width, p_G is the global ice pressure.

In ISO 19906 (2010) and International Electrotechnical Commission (2019), the global ice pressure can be determined as

$$p_G = C_R \left(\frac{h}{h_1}\right)^n \left(\frac{w}{h}\right)^m \tag{7}$$

where C_R is the ice strength coefficient, h_1 is a reference thickness of 1 m, n is an empirical coefficient, equal to $-0.5 + h/5$ for $h < 1.0$ m, and to -0.3 for $h \geq 1.0$ m, m is an empirical coefficient equal to -0.16. The C_R value recommended for Baltic Sea is 1.8 MPa.

In ISO 19906 (2019), the global ice pressure can be determined as

$$p_G = C_R \left[\left(\frac{h}{h_1}\right)^n \left(\frac{w}{h}\right)^m + f_{AR}\right] \tag{8}$$

where f_{AR} is an empirical term given by

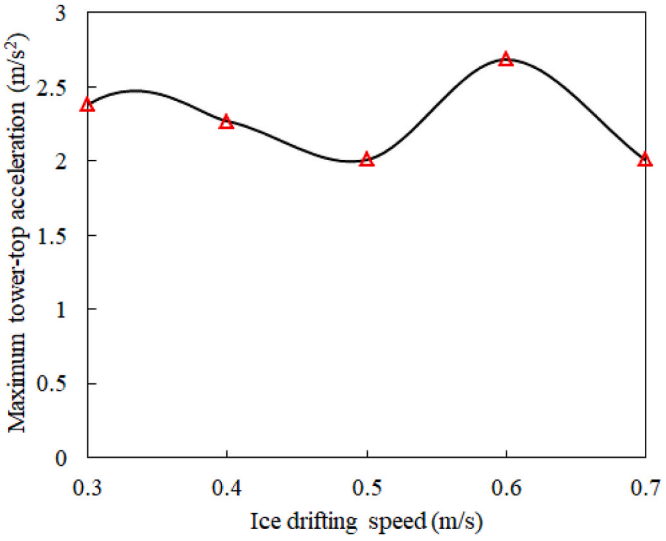

Fig. 16. Variation of the maximum tower-top F-A acceleration with the ice drifting speed.

$$f_{AR} = e^{\frac{-w}{5h}} \sqrt{1 + \frac{5h}{w}} \tag{9}$$

For aspect ratios w/h greater than 5, the f_{AR} term given in Eq. (8) can be disregarded. Therefore, for the case with an OWT diameter of 6 m and ice thickness of 0.4 m, the global ice pressure predicted by ISO 19906 (2019). is equal to that predicted by ISO 19906 (2010).

For a vertical structure with cylindrical shape, International Electrotechnical Commission (2009) recommends the following maximum static force due to crushing as

$$H_d = k_1 k_2 k_3 h D \sigma_c \tag{10}$$

where k_1 is the shape factor equal to 1 for rectangular shape, and to 0.9 for circular shape, k_2 is contact factor equal to 0.5 when the ice is continuously moving, k_3 is aspect ratio factor equal to $\sqrt{1 + 5h/D}$, D is

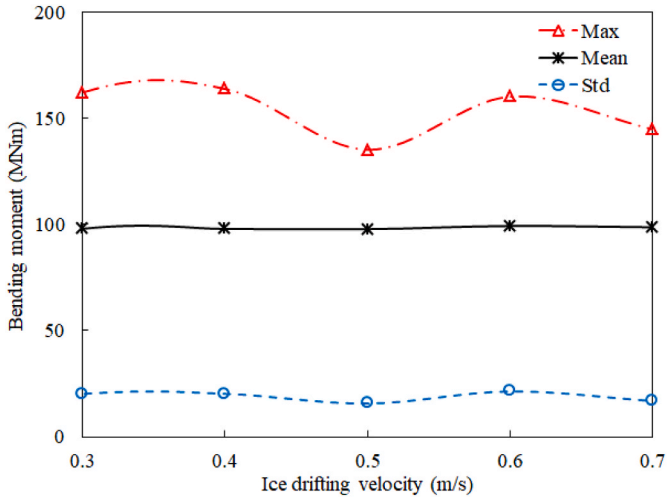

Fig. 17. Variation of the F-A bending moment at the mudline with the ice drifting speed.

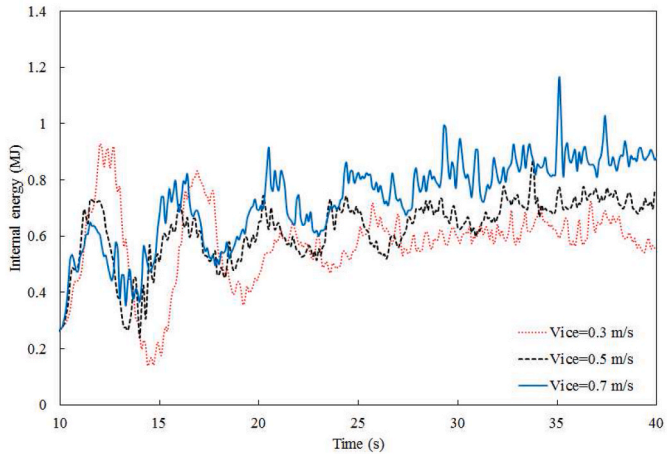

Fig. 18. Time histories of energy dissipation of the OWT under different ice drifting speeds.

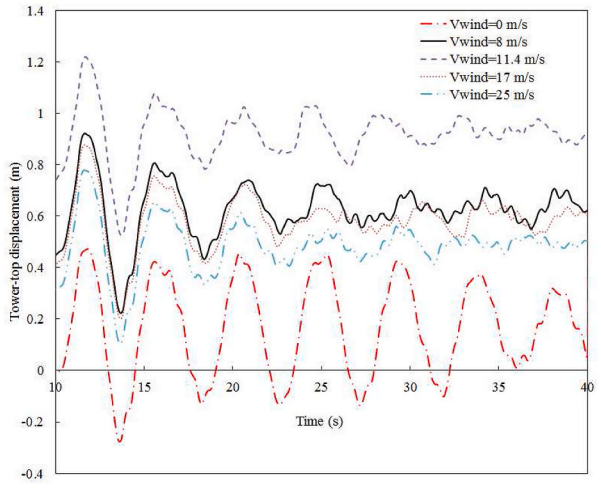

Fig. 19. Time histories of the tower-top F-A displacement for different wind drifting speeds.

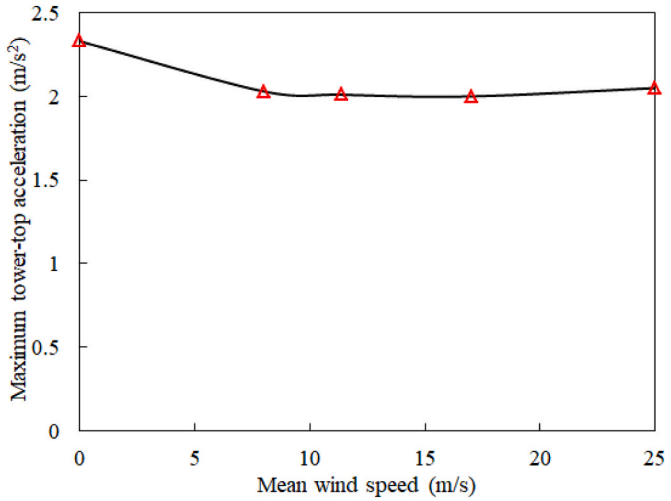

Fig. 20. Variation of the maximum tower-top F-A acceleration with the mean wind speed.

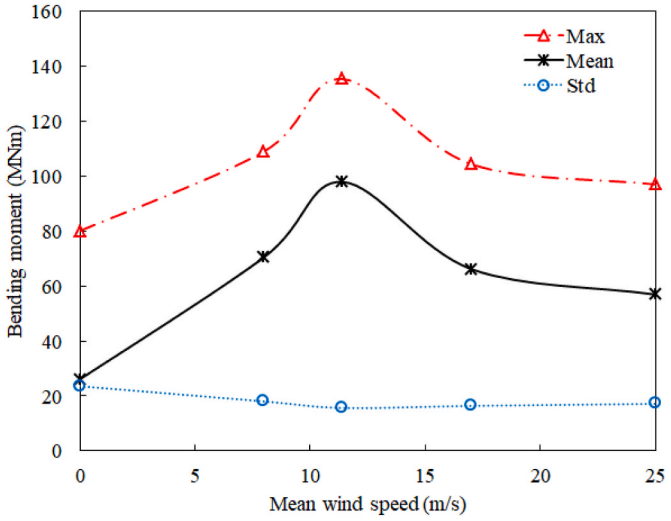

Fig. 21. Variation of the F-A bending moment at the mudline with the mean wind speed.

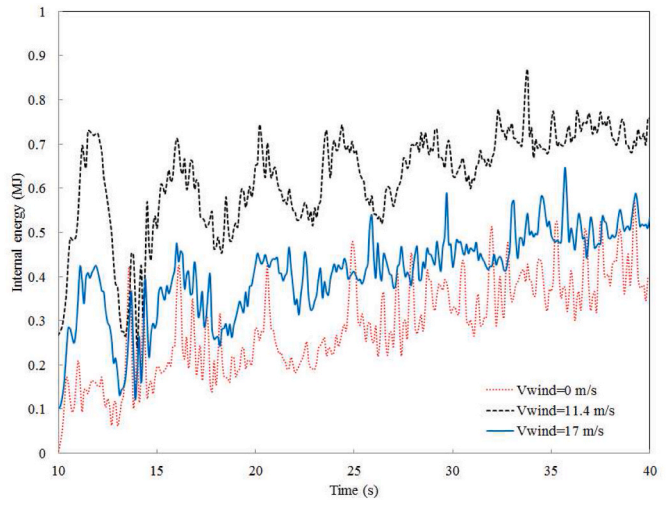

Fig. 22. Time histories of energy dissipation of the OWT for different mean wind speeds.

Table 9
Comparison of standards for estimating ice loads from moving ice onto vertical structures.

Standards	ISO 19906 (2010, 2019) IEC 61400–3 (2019)	IEC 61400–3 (2009)
Structure type	Common offshore structures	Offshore wind turbines
Structure shape	Vertical shapes	Vertical cylindrical shapes
Ice load type	Global load/dynamic load	Static/dynamic loads
Ice failure mode	Crushing	Crushing
Sources	Full-scale measurements in Cook Inlet, the Beaufort Sea, Baltic Sea and Bohai Sea	Measurements in Siberian rivers, and model tests

the diameter of the support structure at the water line, and σ_c is the ice crushing strength.

The dynamic ice load can approximated to vertically shifted sinusoidal as

$$H_{dynv} = H_d\left(\frac{3}{4}+\frac{1}{4}\sin(2\pi f_N t)\right) \tag{11}$$

where t is the time, f_N is the natural frequency of the structure and H_d is the horizontal load from Eq. (10).

The comparison of maximum and mean ice forces for different ice drifting speeds is shown in Fig. 23. The maximum ice force predicted by ISO 19906 (2010, 2019) and International Electrotechnical Commission (2019) with the C_R value of 1.8 MPa is 4.12 MN, which is in the range of the present model predictions. The static and dynamic sin models in International Electrotechnical Commission (2009) yield a lower maximum ice force, while the dynamic sin model yields a much higher mean force. The ice load formula (Eq. (10)) in International Electrotechnical Commission (2009) goes back to Korzhavins Formula (Korzhavin, 1962), which was not intended for offshore structures. Originally the equation for the k_3 factor ($k_3 = \sqrt{1+5h/D}$) was only applied for $1 < D/h < 6$ (GL, 2016), but this is not mentioned in the standard. Hence, its application to the given case ($D/h = 15$) implies an application out of the validity range, which may lead to an underestimation of the maximum load.

Overall, ISO 19906 (2010, 2019) and International Electrotechnical Commission (2019) provide more accurate predictions for the maximum ice load than International Electrotechnical Commission (2009). The predictions using the static or dynamic sinusoidal models of International Electrotechnical Commission (2009) represent a lower bound estimate of the maximum ice force.

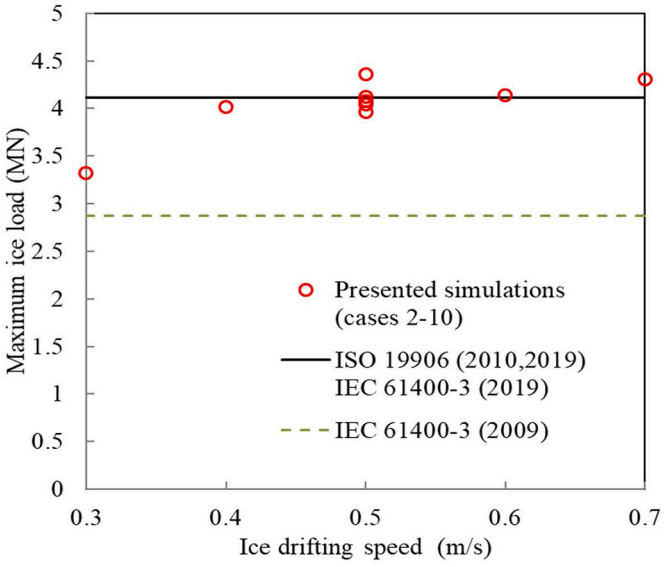

(a)

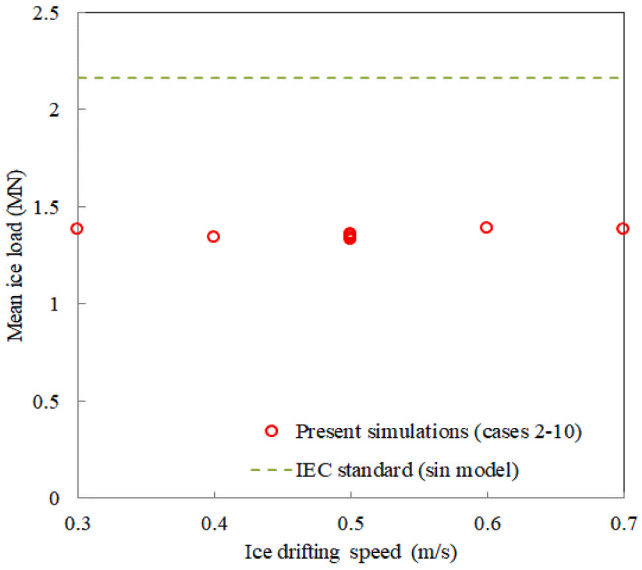

(b)

Fig. 23. Comparison among the simulations (cases 2–10) and the two standards: (a) maximum force, (b) mean force.

6. Discussions

This paper studies the ice-induced loads and dynamic response of a monopole-supported OWT in parked and operating conditions. The continuous brittle crushing mode is considered. These results and limitations of the present study are discussed in the following.

Load cases considered in the present study (cases 2–10) are representative of the design load cases for sea ice (D3 and D8) in International Electrotechnical Commission (2019). For D3, horizontal load from moving ice at relevant velocities and operating wind turbine with the wind speeds in the range of cut-in and cut-out speeds are considered. For D8, horizontal load from moving ice at relevant velocities and parked wind turbine are considered. The ice thickness used in the present study represents the 50-year return period of the Southern Baltic Sea conditions. The maximum ice load during continuous brittle crushing obtained by the present method varies from 3.32 MN to 4.36 MN for the cases 2–10, which agree well with the predictions from ISO 19906 (2010, 2019) and International Electrotechnical Commission (2019). This indicates that the maximum global design load for continuous brittle crushing is reasonable.

The numerical simulations predict significant structural vibrations during the initial stage of the ice impact. The period of the tower oscillations after the initial impact is close to the first eigen period of the OWT. This finding is similar to that in Hammer et al. (2023) who experimentally investigated ice-induced vibrations for an OWT supported by a monopile. In addition, the largest structural stress occurs during the initial ice impact phase; this observation should raise attention for structural design.

The present results show that the mean wind speed has no significant effect on the ice load during continuous brittle crushing. This observation was confirmed by the model test for an idling or operational OWT interacting with sea ice (Hammer et al., 2023).

The ice model used in the present method has limitations and cannot describe all ice failure mechanisms. For ices with low velocities, the ice-structure interaction may turn into frequency lock-in or intermittent

crushing, and such failure modes are not captured by this ice model. Thus, further investigations should be carried out to improve the ice model to describe other ice failure phenomena, especially for low velocities.

From structural design point of view, the key problems involved in the three modes (i.e., intermittent crushing, frequency lock-in and continuous brittle crushing) are totally different. The structural response in the three primary modes of interaction is important primarily for FLS design (ISO 19906, 2019). Frequency lock-in can cause resonant loading and contribute significantly to fatigue accumulation in structures. Multi-modal interaction and intermittent crushing can lead to the largest bending moments in the support structure (Hammer et al., 2023). In future work, the modes of intermittent crushing and frequency lock-in should be focused on.

The studied 5-MW OWT is relatively small in size compared to those of recent commercial OWT projects. Consideration of a larger OWT on the scale of 15-MW OWT will be addressed in future work.

7. Conclusions

In this study, the dynamic response of a monopile-supported offshore wind turbine under combined ice impact and wind load effects is investigated by using the nonlinear finite element method. The ice material model with appropriate mesh size and failure strain is calibrated after a comparison with previous model test data. Based on the calibrated numerical model, various design load cases are considered by a coupled simulation method to investigate the effects of ice impact and wind load on the offshore wind turbine (OWT) responses. In addition, the simulated ice loads are compared to the predictions using the ISO and IEC standards. The conclusions are as follow.

- The simulation considering both the ice impact and wind loads yields larger response of the OWT including the maximum tower-top fore-aft (FA) displacement and the maximum tower bending moments at the MSL and at the mudline, compared to the wind- and ice-only load cases.
- For the ice drifting speed range investigated in this paper (0.3 m/s-0.7 m/s), a negligible effect of the ice drifting speed is found on the mean ice force, the mean tower-top displacement and the mean F-A bending moment at the mudline. Still, the ice drifting speed has a significant effect on the maximum tower-top displacement, the tower oscillation period and the energy dissipation. The maximum tower-top displacement and the tower oscillation period decrease with the increase of the ice drifting speed. The energy dissipated by the OWT shows a growing trend as the ice drifting speed increases.
- The mean wind speed significantly affects the tower-top displacement, the energy dissipation, and the F-A bending moment at the mudline. The largest response of the OWT is attained when the mean wind speed is equal to rated (11.4 m/s). The maximum tower-top displacement and the maximum F-A bending moment at the mudline for a mean wind speed of 11.4 m/s are approximately 2.58 and 1.69 times than those obtained without considering wind loads. But, the mean wind speed has a little effect on the ice force.
- For the maximum ice load, ISO 19906 (2010, 2019) and International Electrotechnical Commission (2019) provide predictions that agree well with those obtained by the proposed method, whereas International Electrotechnical Commission (2009) gives a lower bound estimate. The ISO standard for the prediction of maximum ice load is recommended.

CRediT authorship contribution statement

Ming Song: Conceptualization, Methodology, Investigation, Writing – original draft, contributed to concept contruction, research methodology, investigation, and writing. **Zhiyu Jiang:** Methodology, Writing – original draft, contributed to research methodology, results discussion, and writing. **Kun Liu:** Writing – review & editing, contributed to discussion, writing and review. **Yue Han:** Writing – review & editing, contributed to discussion, writing and review. **Renwei Liu:** Writing – review & editing, contributed to discussion, writing and review.

Data availability

Data will be made available on reasonable request.

Acknowledgements

This work has been financially supported by the National Key Research and Development Program (Grant No. 2022YFE0107000); Natural Science Foundation of Jiangsu Province of China (Grant No. BK20200998); National Natural Science Foundation of China (Grant Nos. 52171311, 52271279, 51579130, 52201323). The first author also acknowledges the visiting scholar scholarship provide by University of Agder, Norway. The second author acknowledges the financial support from ImpactWind SouthWest (RCN Project No. 332034).

References

API, 1995. Recommended Practice for Planning, Designing, and Constructing Structures and Pipelines for Arctic Conditions. American Petroleum Institute.
Bachynski, E.E., 2014. Design and Dynamic Analysis of Tension Leg Platform Wind Turbines. PhD thesis Norwegian University of Science and Technology.
Barker, A., Timco, G., Gravesen, H., Vølund, P., 2005. Ice loading on Danish wind turbines: part 1: dynamic model tests. Cold Reg. Sci. Technol. 41 (1), 1–23.
Barooni, M., Nezhad, S., Ali, N., Ashuri, T., Sogut, D., 2022. Numerical study of ice-induced loads and dynamic response analysis for floating offshore wind turbines. Mar. Struct. 86, 103300.
Berg, M., Owen, C., Hendrikse, H., 2022. Experimental study on ice-structure interaction phenomena of vertically sided structures. Cold Reg. Sci. Technol. 201.
CAN/CSA S471-04, 2004. General Requirements, Design Criteria, the Environment, and Loads. Canadian Standards Association.
DNV-GL, 2016. Loads and Site Conditions for Wind Turbines. Standard DNVGL-ST-0437.
Germanischer, Lloyd, 2016. Guideline for the Construction of Fixed Offshore Installations in Ice Infested Waters. Rules & Guidelines.
Gravesen, H., Sørensen, S.L., Vølund, P., Barker, A., Timco, G., 2005. Ice loading on Danish wind turbines: Part 2. Analyses of dynamic model test results. Cold Reg. Sci. Technol. 41 (1), 25–47.
Gürtner, A., Bjerkas, M., Kuhnlein, W., Jochmann, P., Konuk, I., 2009. Numerical simulation of ice action to a lighthouse. In: Proceedings of the 28th International Conference on Ocean, Offshore and Arctic Engineering (OMAE), Honolulu, HI, USA. , 31 May–5 June.
Hallquist, J.O., 2013. LS-DYNA User's Manuals Version 971, vols. 1 & 2.
Hammer, T.C., Willems, T., Hendrikse, H., 2023. Dynamic ice loads for offshore wind support structure design. Mar. Struct. 87, 103335.
Heinonen, J., Rissanen, S., 2017. Coupled-crushing analysis of a sea ice-wind turbine interaction-feasibility study of FAST simulation software. Ships Offshore Struct. 1–8.
Hendrikse, H., Nord, T., 2019. Dynamic response of an offshore structure interacting with an ice floe failing in crushing. Mar. Struct. 65, 271–290.
Hilding, D., Forsberg, J., Gürtner, A., 2011. Simulation of Ice Action Loads on Offshore Structures. 8th European LS-DYNA Users Conference, Strasbourg, France, pp. 1–12.
International Electrotechnical Commission, 2009. IEC. Wind Turines, Part 3: Design Requirements for Offshore Wind Turbines 61400-3.
International Electrotechnical Commission, 2019. IEC. Wind Turines, Part 3: Design Requirements for Offshore Wind Turbines 61400-3.
International organization for standardization, ISO 19906, 2010. Petroleum and Natural Gas Industries-Arctic Offshore Structures.
International organization for standardization, ISO 19906, 2019. Petroleum and Natural Gas Industries-Arctic Offshore Structures.
Ji, S., Yang, D., 2022. Ice loads and ice-induced vibrations of offshore wind turbine based on coupled DEM-FEM simulations. Ocean. Eng. 110–197.
Jonkman, J., Butterfield, S., Passon, P., Larsen, T., Camp, T., Nichols, J., Azcona, J., Martinez, A., 2007. Offshore Code Comparison Collaboration within IEA Wind Annex XXIII: Phase II Results, vol. 12. IEA European Offshore Wind Conference, Berlin, Germany, pp. 4–6.
Kellner, L., Herrnring, H., Ring, M., 2017. Review of ice load standards and comparison with measurements. Proceedings of the ASME 2017 36th International Conference on Ocean, Offshore and Arctic Engineering 6, 25–30 (Trondheim, Norway).
Korzhavin, K., 1962. Action of Ice on Engineering Structures. Transl. U.S. Joint Publications Research Service, U.S. Army Cold Regions Research and Engineering Laboratory, Hanover.
Kuutti, J., Kolari, K., Marjavaara, P., 2013. Simulation of ice crushing experiments with cohesive surface methodology. Cold Reg. Sci. Technol. 92, 17–28.
Larsen, T.J., Hansen, A.M., 2018. How 2 HAWC2, the user's manual. Risø-R 1597 ver. 4-7).

Li, F., Tian, P., Wang, L.X., Chen, M.S., 2020. Investigation on lateral bearing capacity of monopile under combined vertical-lateral loads and scouring condition. Mar. Georesour. Geotechnol. 39 (4), 505–514.
Liu, C., Hao, E., Zhang, S., 2015. Optimization and application of a crashworthy device for the monopile offshore wind turbine against ship impact. Appl. Ocean Res. 51, 129–137.
Määttänen, M., 2010. Ice research and engineering in Finland. In: Proceedings of the 20th International Symposium on Ice (IAHR)., vol. 6 Lahti, pp. 14–18.
Määttänen, M., Marjavaara, P., Saarinen, S., Laakso, M., 2011. Ice crushing tests with variable structural flexibility. Cold Reg. Sci. Technol. 67 (3), 120–128.
NORSOK N-003, 2007. Actions and Action Effects. Norwegian Technology Standards, Oslo.
Sanderson, T.J.O., 1988. Ice Mechanics: Risks to Offshore Structures. Graham and Trotman, London, p. 253, 0-86010-785-X.
Seidel, M., Hendrikse, H., 2018. Analytical assessment of sea ice-induced frequency lock-in for offshore wind turbine monopoles. Mar. Struct. 60, 87–100.
Shi, W., Tan, X., Gao, Z., Moan, T., 2016. Numerical study of ice-induced loads and responses of a monopile-type offshore wind turbine in parked and operating conditions. Cold Reg. Sci. Technol. 123, 121–139.
Shi, W., Liu, Y.Z., Wang, W.H., Cui, L., Li, X., 2023. Numerical study of an ice-offshore wind turbine structure interaction with the pile-soil interaction under stochastic wind loads. Ocean. Eng. 273, 113984.
Song, M., Kim, E., Amdahl, J., Ma, J., Huang, Y., 2016. A comparative analysis of the fluid-structure interaction method and the constant added mass method for ice-structure collisions. Mar. Struct. 49, 58–75.
Song, M., Shi, W., Ren, Z., Zhou, L., 2019. Numerical study of the interaction between level ice and wind turbine tower for estimation of ice crushing loads on structure. J. Mar. Sci. Eng. 7 (12), 1–23.
Song, M., Jiang, Z., Yuan, W., 2021. Numerical and analytical analysis of a monopile-supported offshore wind turbine under ship impacts. Renew. Energy 167, 457–472.
Wang, F., Zou, Z., Zhou, L., Ren, Y., Wang, S., 2018. A simulation study on the interaction between sloping marine structure and level ice based on cohesive element model. Cold Reg. Sci. Technol. 149, 1–15.
WindEurope, 2019. Boosting Offshore Wind Energy in the Baltic Sea.
Wu, H., Huang, Y., Li, W., 2018. Experimental study on the ice load of large-diameter monopile wind turbine foundations. Ocean. Eng. 36, 83–91.
Yue, Q., Guo, F., Kärnä, T., 2009. Dynamic ice forces of slender vertical structures due to ice crushing. Cold Reg. Sci. Technol. 56 (2), 77–83.
Zhu, L., Liu, Q., Jones, N., Chen, M., 2018. Experimental study on the deformation of fully clamped pipes under lateral impact. Int. J. Impact Eng. 111, 94–105.
Zhu, L., Cai, W., Chen, M.S., Tian, Y.K., Bi, L.Z., 2020. Experimental and numerical analyses of elastic-plastic responses of ship plates under ice floe impacts. Ocean. Eng. 218, 108174.